Dominant Fifth-Order Correlations in Doped Quantum Antiferromagnets

A. Bohrdt,[1,2] Y. Wang,[3,4] J. Koepsell,[5,2] M. Kánasz-Nagy,[5] E. Demler,[3] and F. Grusdt[6,2]
[1]Department of Physics and Institute for Advanced Study, Technical University of Munich, 85748 Garching, Germany
[2]Munich Center for Quantum Science and Technology (MCQST), Schellingstrasse 4, D-80799 München, Germany
[3]Department of Physics, Harvard University, Cambridge, Massachusetts 02138, USA
[4]Department of Physics and Astronomy, Clemson University, Clemson, South Carolina 29631, USA
[5]Max-Planck-Institut für Quantenoptik, 85748 Garching, Germany
[6]Department of Physics and Arnold Sommerfeld Center for Theoretical Physics (ASC), Ludwig-Maximilians-Universität München, Theresienstrasse 37, München D-80333, Germany

(Received 11 August 2020; accepted 11 December 2020; published 12 January 2021)

Traditionally, one- and two-point correlation functions are used to characterize many-body systems. In strongly correlated quantum materials, such as the doped 2D Fermi-Hubbard system, these may no longer be sufficient, because higher-order correlations are crucial to understanding the character of the many-body system and can be numerically dominant. Experimentally, such higher-order correlations have recently become accessible in ultracold atom systems. Here, we reveal strong non-Gaussian correlations in doped quantum antiferromagnets and show that higher-order correlations dominate over lower-order terms. We study a single mobile hole in the $t-J$ model using the density matrix renormalization group and reveal genuine fifth-order correlations which are directly related to the mobility of the dopant. We contrast our results to predictions using models based on doped quantum spin liquids which feature significantly reduced higher-order correlations. Our predictions can be tested at the lowest currently accessible temperatures in quantum simulators of the 2D Fermi-Hubbard model. Finally, we propose to experimentally study the same fifth-order spin-charge correlations as a function of doping. This will help to reveal the microscopic nature of charge carriers in the most debated regime of the Hubbard model, relevant for understanding high-T_c superconductivity.

DOI: 10.1103/PhysRevLett.126.026401

Introduction.—High-temperature superconductors are prime examples of strongly correlated quantum matter. In these quasi-2D systems, superconductivity arises when mobile dopants are introduced into a parent antiferromagnetic (AFM) compound [1,2], but the detailed mechanism remains elusive. It is widely believed that the interplay of spin and charge degrees of freedom plays a central role for understanding the underlying physics at low doping and can be described theoretically by the Fermi-Hubbard or $t-J$ model [3]. The central goal of this Letter is to demonstrate that key features of magnetic dressing of doped holes in the Fermi-Hubbard model can be revealed by analyzing five-point spin-charge correlation functions. Furthermore, such high-order correlation functions are found to be larger than the lower-order ones in the regime of low doping and low temperatures.

Understanding the nature of charge carriers in strongly correlated electron systems, such as the doped Fermi-Hubbard model, is a central problem of quantum many-body physics. While a single mobile hole inside the 2D quantum-Heisenberg AFM forms a magnetic (or spin) polaron [4–16], with spin and charge quantum numbers, it remains unknown whether spin and charge excitations (spinons and chargons, respectively) may become deconfined in the strange metal and pseudogap regimes, usually a characteristic of doped 1D spin chains [17–20]. Direct experimental or numerical evidence remains lacking so far.

A common perspective on the puzzling properties of cuprates is the idea of several competing orders. Thus, numerical studies of the Fermi-Hubbard and $t-J$ models have often focused on the analysis of two-point correlation functions, which also allow one to characterize different types of broken symmetries. Furthermore, two-point correlation functions can be naturally accessed in solid state systems using scattering experiments [21–23], and they play a central role in the development of effective mean-field theories. Recently, with the advent of quantum simulators based on ultracold atoms and ions and, especially, quantum gas microscopes [24–31], analysis of higher-order correlation functions, pioneered in Ref. [32], has become a new experimental tool in the study of quantum many-body states [14,33–38]. They have rarely been studied so far, even though they contain a wealth of information about the underlying quantum states and are expected to become relevant when mean-field theories characterized by Gaussian correlations are no longer sufficient for capturing the physics. A notable exception is constituted by three-point spin-charge correlations, which have previously been

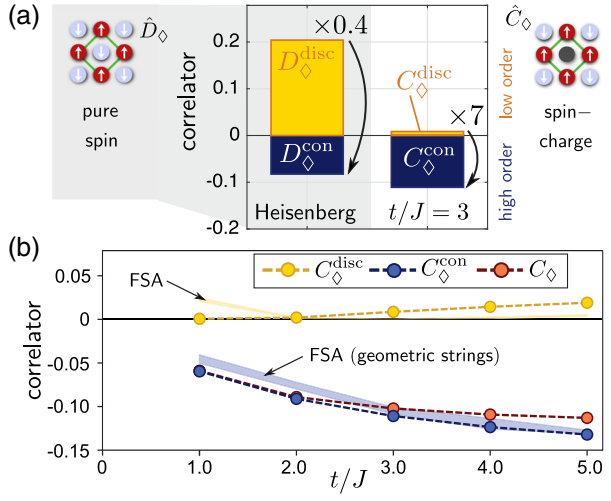

FIG. 1. Fifth-order spin-charge correlations in a quantum AFM with a mobile dopant are studied in the 2D $t-J$ model and compared to the corresponding fourth-order correlators in the undoped Heisenberg AFM (a). We use the density matrix renormalization group (DMRG) on a 6×12 cylinder and evaluate correlators at the center, in spin-balanced ensembles with $\langle \hat{S}^z\rangle = 0$. For one mobile dopant, genuine fifth-order correlations $C_\diamond^{\mathrm{con}}$ [Eq. (2), blue] are significantly larger (by a factor $\times 7$) than the lower-order disconnected terms $C_\diamond^{\mathrm{disc}} = C_\diamond - C_\diamond^{\mathrm{con}}$ (yellow). In the undoped Heisenberg AFM, the opposite is true: Lower-order correlators are dominant, while genuine higher-order correlations are smaller ($\times 0.4$). (b) Spin-charge correlators as a function of t/J. Our numerical results (data points, bare correlations $C_\diamond$ in red) are explained by a FSA ansatz (ribbons; width indicates statistical errors).

theoretically analyzed [15,39–42] and recently been measured [14].

Here, we identify lightly doped quantum AFMs as a system where genuine higher-order spin-charge correlations are present. Different from the situation in the undoped parent spin models, these higher-order correlations even dominate over lower-order (including three-point) terms when t/J is sufficiently large; see Fig. 1(a). Hence, they provide a promising new diagnostic to unravel the nature of charge carriers and distinguish different many-body states [43]. Indeed, we show that even nonperturbative effective descriptions, such as doped resonating valence bond (RVB) states, cannot explain the higher-order correlations we find numerically at low doping. Instead, our results can be interpreted as signatures of geometric strings [15,44] connecting spinons and chargons [45–48], reminiscent of an underlying $\mathbb{Z}_2$ Gauss law. Physically, strong five-point correlations indicate that a moving hole leaves behind a string of flipped spins, as shown in Fig. 2.

In this Letter, after introducing the higher-order spin-charge correlators, we perform DMRG ground state simulations of one mobile dopant on an extended cylinder. We then compare the latter to effective theoretical descriptions based on doped RVB states and the string picture. Finally,

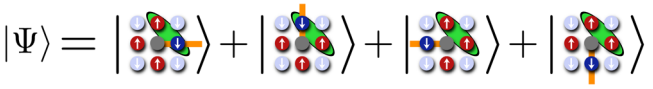

FIG. 2. The three-point spin-charge correlator diagonally next to the hole, $\langle \hat{n}_j^h \hat{S}^z_{j+e_x} \hat{S}^z_{j+e_y}\rangle$ (green bubble next to gray dot), vanishes for a mobile hole moving through a classical Néel state at the end of an S^z string of length $\ell \geq 1$. The fifth-order correlations $C_\diamond \propto \langle \hat{n}_j^h \hat{S}^z_{j+e_x} \hat{S}^z_{j+e_y} \hat{S}^z_{j-e_x} \hat{S}^z_{j-e_y}\rangle$ remain sizable and negative.

we use exact diagonalization to determine the temperature required for an experimental verification. In a follow-up paper, we include the effect of a pinning potential [49].

Higher-order correlators.—We consider the following fifth-order ring spin-charge correlator:

$$C_\diamond(\boldsymbol{r}) = \frac{2^4}{\langle \hat{n}^h_{\mathbf{r}}\rangle} \langle \hat{n}^h_{\boldsymbol{r}} \hat{S}^z_{\boldsymbol{r}+e_x} \hat{S}^z_{\boldsymbol{r}+e_y} \hat{S}^z_{\boldsymbol{r}-e_x} \hat{S}^z_{\boldsymbol{r}-e_y}\rangle, \tag{1}$$

where $\hat{n}^h_{\boldsymbol{r}}$ is the hole (dopant) density at site $\boldsymbol{r}$ and $\hat{S}^z_{\boldsymbol{j}}$ denotes the spin operator in the z direction at site $\boldsymbol{j}$. To witness the presence of genuine higher-order correlations, we calculate the connected correlator in the comoving frame with the hole (defined in Supplemental Material [50]). In a spin-balanced ensemble with $\langle \hat{S}^z\rangle = 0$ (see discussion in Ref. [49]), expectation values with an odd number of $\hat{S}^z$ operators vanish, and we obtain

$$C_\diamond^{\mathrm{con}} = C_\diamond - 2^4 \sum_{(i,j)\notin(k,l)} \frac{\langle \hat{n}^h_{\boldsymbol{r}} \hat{S}^z_{\boldsymbol{r}+i} \hat{S}^z_{\boldsymbol{r}+j}\rangle}{\langle \hat{n}^h_{\mathbf{r}}\rangle} \frac{\langle \hat{n}^h_{\boldsymbol{r}} \hat{S}^z_{\boldsymbol{r}+k} \hat{S}^z_{\boldsymbol{r}+l}\rangle}{\langle \hat{n}^h_{\mathbf{r}}\rangle}. \tag{2}$$

In weakly correlated quantum systems, the values of higher-order correlation functions are dominated by more fundamental lower-order correlators; i.e., connected nth-order correlation functions C_n^{con} decrease with decreasing n, $|C_1^{\mathrm{con}}| > |C_2^{\mathrm{con}}| > \cdots$. For classical (product) states all connected correlations vanish $C_n^{\mathrm{con}} = 0$, while in Gaussian systems only $C_1^{\mathrm{con}}, C_2^{\mathrm{con}} \neq 0$ are nonzero [51].

Magnetic polarons.—Intriguingly, for a magnetic polaron, formed when a single mobile hole is doped into an AFM, we find that the disconnected contributions from the lower-order correlators, $C_\diamond^{\mathrm{disc}} = C_\diamond - C_\diamond^{\mathrm{con}}$, are significantly *smaller* in magnitude than the higher-order correlators: $|C_\diamond^{\mathrm{disc}}| > |C_\diamond(\boldsymbol{r})|, |C_\diamond^{\mathrm{con}}(\boldsymbol{r})|$. In Fig. 1, we show DMRG results [52] for the ground state of a single hole in the $t-J$ [53] model, as a function of t/J. The mobility of the dopant plays an important role for observing sizable higher-order spin-charge correlations. As t/J is increased from $t/J = 1$ to $t/J = 5$, the absolute value of $C_\diamond^{\mathrm{con}}$ approximately doubles. Throughout, the product of the lower-order two-point correlation functions is almost an order of magnitude smaller.

We can define related fourth-order correlators in the absence of doping as $D_\diamond(\boldsymbol{r}) = 2^4\langle \hat{S}^z_{\boldsymbol{r}+\boldsymbol{e}_x}\hat{S}^z_{\boldsymbol{r}+\boldsymbol{e}_y}\hat{S}^z_{\boldsymbol{r}-\boldsymbol{e}_x}\hat{S}^z_{\boldsymbol{r}-\boldsymbol{e}_y}\rangle$; a corresponding expression is obtained for the connected part $D^{\mathrm{con}}_\diamond(\boldsymbol{r})$. In the classical Ising AFM, $D_\diamond = 1$ and $D^{\mathrm{con}}_\diamond = 0$. For the 2D Heisenberg model, we performed DMRG simulations on a 6×12 cylinder and obtained $D_\diamond = 0.12$ and $D^{\mathrm{con}}_\diamond = -0.083$ in the ground state, as indicated in Fig. 1(a). The connected fourth-order correlator becomes negative only because we subtract the significantly larger and positive two-point correlators, $D^{\mathrm{disc}} = D_\diamond - D^{\mathrm{con}}_\diamond = 0.20$. As expected for a weakly correlated quantum system and different from the ground state with a mobile hole in the $t-J$ model, the lower-order correlators dominate in the 2D Heisenberg model: They are more than twice as large as the genuine fourth-order correlations.

Orders of magnitude and the signs of $D^{(\mathrm{con})}_\diamond$ can be understood from a simple model of spontaneous symmetry breaking. Consider an ensemble of classical Néel states with AFM order parameters pointing in random directions. Because $D_\diamond$ is always measured in the z basis, we average over the entire ensemble and obtain

$$D_\diamond|_{\mathrm{cl}} = 0.2, \qquad D^{\mathrm{con}}_\diamond|_{\mathrm{cl}} = -0.133. \tag{3}$$

These correlations are purely classical. Quantum fluctuations are expected to further reduce these values in the SU(2)-invariant Heisenberg model, as confirmed by our DMRG calculations.

Geometric and S^z strings.—Negative fifth-order correlations $C^{\mathrm{con}}_\diamond(\boldsymbol{r}) < 0$ provide a signature of AFM correlations hidden by the motion of dopants. To understand the origin of such higher-order correlations, we first consider a toy model of a single hole in an Ising AFM pointing along the S^z direction. Neglecting string configurations affecting more than one spin in the direct vicinity of the mobile dopant, we notice that $C_\diamond$ switches sign if the hole is attached to a string Σ of overturned spins (S^z string) of length $\ell > 0$. Hence, $C_\diamond$ can be expressed by the probability $p_{\ell>0}$ for the string to have nonzero length, namely, $C_\diamond \approx p_{\ell=0} - p_{\ell>0}$ or $C_\diamond \approx 1\text{–}2p_{\ell>0}$.

Assuming that the system is in an equal superposition of all string configurations, we can estimate various correlation functions. Because the hole is equally likely to occupy either sublattice, $\langle \hat{n}^h_{\boldsymbol{r}}\hat{S}^z_{\boldsymbol{r}\pm\boldsymbol{e}_{x,y}}\rangle = 0$. Three-point correlations $\langle \hat{n}^h_{\boldsymbol{r}}\hat{S}^z_{\boldsymbol{r}\pm\boldsymbol{e}_{x,y}}\hat{S}^z_{\boldsymbol{r}\pm\boldsymbol{e}_{x,y}}\rangle = 0$ vanish, as can be seen by averaging over the four possible orientations of the first string segment, counting from the hole, and neglecting string configurations which affect more than one spin in the immediate vicinity of the hole; see Fig. 2. Hence, $C^{\mathrm{con}}_\diamond(\boldsymbol{r}) = C_\diamond(\boldsymbol{r}) \approx -1$ for sufficiently many nonzero strings $p_{\ell>0} \approx 1$.

In this setting, relevant to the 2D $t-J_z$ model [44,54], $C_\diamond$ takes the role of a $\mathbb{Z}_2$ Gauss law: The mobile dopants represent $\mathbb{Z}_2$ charges, and the $\mathbb{Z}_2$ electric field lines correspond to S^z strings of overturned spins. Similarly, in the SU(2)-invariant $t-J$ or Fermi-Hubbard models, the higher-order correlator $C_\diamond$ serves as an indicator for geometric strings [15,44] of displaced spins.

The t/J dependence observed in Fig. 1 can be explained within the geometric string theory by a frozen-spin approximation (FSA) ansatz [44]. As in Refs. [55,56], we start from snapshots of the Heisenberg ground state in the Fock basis along S^z and create a hole by randomly removing one spin. This dopant is subsequently moved through the system in random directions, rearranging the positions of the surrounding spins while keeping their quantum state frozen; the string length distribution is calculated from a linear string model with string tension $dE/d\ell = 2J(C_2 - C_1)$ [44], where $C_{1(2)}$ are nearest (next-nearest) neighbor spin correlations in the undoped AFM. This way, new sets of snapshots are generated for every value of t/J, from which the higher-order correlators can then be obtained [55].

Doped spin liquids.—A class of microscopic variational wave functions that has been used to model doped quantum spin liquids is based on Anderson's RVB paradigm [57,58]. Being able to resolve properties of the many-body wave function on microscopic scales, ultracold atom experiments provide an opportunity to put the RVB theory to a rigorous experimental test in a clean system.

Here, we calculate the higher-order spin-charge correlations $C^{(\mathrm{con})}_\diamond$ for two paradigmatic doped RVB trial states. The uniform RVB state starts from an unpolarized Fermi sea $|\mathrm{FS}\rangle$ of free spin-up and spin-down spinons $\hat{f}_{\boldsymbol{k},\sigma}$. To describe a free hole excitation moving through the system, one spinon with momentum $\boldsymbol{k}$ and spin σ is removed. A meaningful trial state for the $t-J$ model, without double occupancies and independent of t/J, is obtained by applying the Gutzwiller projection: $|\Psi_{\mathrm{uRVB}}\rangle = \mathcal{N}\hat{\mathcal{P}}_{\mathrm{GW}}\hat{f}_{\boldsymbol{k},\sigma}|\mathrm{FS}\rangle$ normalized by $\mathcal{N}$. We use standard Metropolis Monte Carlo sampling [59] to evaluate $C^{(\mathrm{con})}_\diamond$ in the trial state $|\Psi_{\mathrm{uRVB}}\rangle$ and show our result in Fig. 3. We find $C^{(\mathrm{con})}_\diamond = -0.040(4)$ with significantly smaller magnitude than found for large values of t/J by DMRG; cf. Fig. 1.

We find a similar result for the doped π-flux RVB state [60], for which decent agreement with experimental data has recently been reported in ultracold atoms at finite doping [55,56]. The π-flux state with a single hole has the same form as the uRVB state above, except that the Fermi sea $|\mathrm{FS}\rangle$ is replaced by a Dirac semimetal of spinons obtained when introducing π magnetic flux per plaquette in the effective spinon Hamiltonian [61]. In this case, $C^{\mathrm{con}}_\diamond = -0.049(3)$ slightly increases and $C_\diamond = -0.008(3)$ decreases in magnitude. Both are significantly weaker than numerically expected from DMRG when $t > J$.

In a recently proposed extension of the RVB ansatz, geometric strings are included in the trial wave function [15,62]. Now we demonstrate that the presence of such

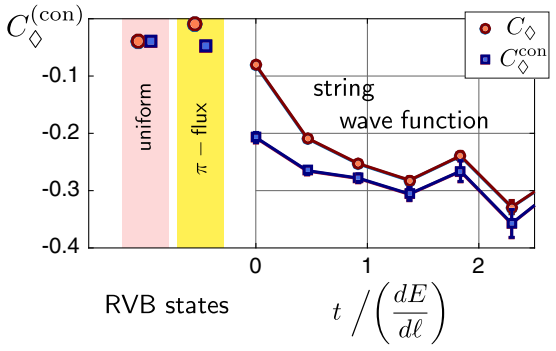

FIG. 3. Comparison of RVB and geometric string trial states in a 14×14 system with $S^z_{\mathrm{tot}} = 1/2$. For the "plain vanilla"uniform and π-flux RVB states doped with a single hole (left), $C_\diamond^{(\mathrm{con})}$ is small. The string wave function (right), with a weak SU(2)-breaking staggered magnetization along S^z, exhibits larger values of the spin-charge correlator and shows a strong dependence on the ratio of t and the string tension $dE/d\ell = 1.09J$ [15], which determines the average length of geometric strings in the trial state. Note that the doped RVB states have no t/J dependence.

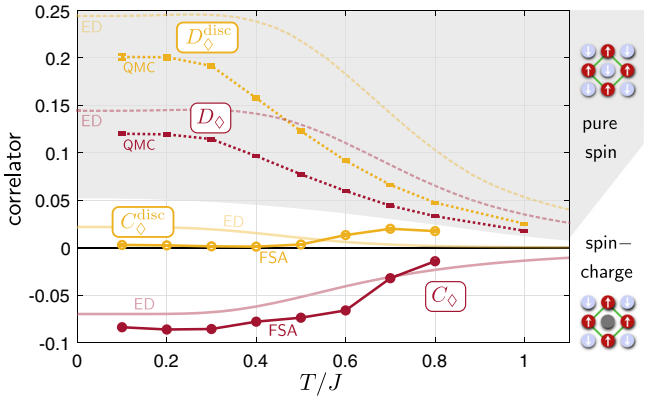

FIG. 4. Temperature dependence of the higher-order correlations $C_\diamond$ (red lines) and the disconnected $C_\diamond^{\mathrm{disc}}$ (yellow lines) parts [using Eq. (2)]. We compare the corresponding correlators $D_\diamond$ in the undoped Heisenberg model (top) to predictions for a mobile dopant (with $t/J = 2$), using the FSA in a 16×16 lattice based on Heisenberg quantum Monte Carlo (QMC) snapshots, and ED simulations in a periodic 4×4 system.

geometric strings increases the expected higher-order correlators. We start from the optimized RVB wave function for half filling (no doping) [63,64], which includes a weak spontaneously formed staggered magnetization along the S^z direction. A spinon is removed in the usual way, and after the Gutzwiller projection a geometric string is added to the hole, thus rearranging the spins surrounding the dopant; see Refs. [15,62] for details.

In Fig. 3 (right panel), we show how $C_\diamond^{(\mathrm{con})}$ evaluated for this string wave function depends on the ratio of hole tunneling t and the linear string tension $dE/d\ell$ underlying the model. When $t/J = 0$, the length of geometric strings is zero, and the observed increase of the higher-order correlator is due to the staggered magnetization along S^z included in the trial wave function. For increasing tunneling t, the string length grows and another significant increase of $C_\diamond^{(\mathrm{con})}$ is observed. This supports our picture that the mobility of dopants leads to long geometric strings, which, in turn, underly strong higher-order spin-charge correlations.

Experimental considerations.—We turn to a discussion of the limitations and requirements to observe higher-order correlations in the doped Hubbard model.

Figure 4 demonstrates how thermal fluctuations suppress higher-order correlations. We show the lower-order disconnected terms $C_\diamond^{\mathrm{disc}}$ and compare them to the higher-order correlators $C_\diamond$, in two cases: For the undoped Heisenberg model, we use quantum Monte Carlo simulations [65]. For a single mobile dopant, our predictions are based on the frozen-spin approximation (FSA and geometric strings) [44,55,56] described above. The correlators are evaluated from 10^4 snapshots for each T/J. We also compare to exact diagonalization (ED) calculations in a 4×4 system and find good agreement.

In the geometric string theory, $C_\diamond^{\mathrm{disc}}$ is approximately zero up to temperatures $T \lesssim 0.5J$, while the higher-order correlator $C_\diamond$ is of the order of -0.1. Without a hole, the disconnected part $D_\diamond^{\mathrm{disc}}$ is significantly larger than $D_\diamond$ for these small temperatures. For $T \gtrsim 0.6J$, the correlations decay quickly. The relevant temperature range has already been accessed experimentally [66], and we expect that more quantum gas microscopes operating in this regime will follow in the near future [27,29,34,67,68]. Similar to quantum gas microscopy, the higher-order correlations in Fig. 4 are extracted from snapshots. We expect that the main experimental challenge will be to collect sufficient amounts of data to obtain acceptable error bars. Current experiments offering simultaneous spin and charge resolution [36] are very close to the temperature regime required for observing the higher-order correlations proposed here.

Summary and outlook.—We propose to study fifth-order spin-charge correlations to explore the microscopic nature of charge carriers in the doped Hubbard model from a new perspective. Such correlators have recently become accessible in state-of-the-art quantum gas microscopes. The observables we consider are direct generalizations of the three-point spin-charge correlators $\langle \hat{S}^z_{j-1} \hat{n}^h_j \hat{S}^z_{j+1} \rangle$ underlying hidden AFM correlations in the 1D doped Hubbard model [69,70]. We analyze similar correlations in 2D, which can be understood only by theories with non-Gaussian correlations.

Our numerical studies for a single doped hole reveal the importance of the hole mobility for establishing such higher-order correlations and making them become the dominant spin-charge correlations in the system. In a subsequent work, we demonstrate this explicitly by considering the effect of a localized pinning potential for the hole [49]. Here, we also established that doped quantum

spin liquids have reduced higher-order correlations, whereas fluctuating geometric strings can explain the observed enhancement when t/J is increased.

An interesting question concerns the behavior of the higher-order correlations when doping is increased and numerical studies of the Fermi-Hubbard model become more challenging [71]. In this regime, we propose to measure the higher-order correlators by state-of-the-art ultracold atom experiments. Such studies can shed new light on the nature of charge carriers in the pseudogap and strange-metal [72] regimes or the pairing mechanism between dopants. They also provide a new experimental route to distinguish theoretical trial states, e.g., in the RVB class. While a recent machine-learning analysis [56] suggests that up to $\simeq 15\%$ doping a model based on geometric strings may be favorable compared to doped π-flux RVB states, further refined experiments as proposed here will be required to establish where and how the nature of charge carriers changes upon doping.

Our results can be applied to extend studies of the formation dynamics of magnetic polarons [73–75] or to investigate correlation effects in Bose polaron problems in an optical lattice [76]. Other possible extensions include the study of SU(2)-invariant generalizations of the higher-order spin-charge correlators introduced here.

The authors thank T. Hilker, T. Zache, M. Prüfer, M. Knap, D. Sels, P. Preiss, S. Jochim, and I. Bloch for useful discussions. We acknowledge funding by the Deutsche Forschungsgemeinschaft (DFG, German Research Foundation) under Germany's Excellence Strategy—EXC-2111-390814868. Y. W. acknowledges the Postdoctoral Fellowship of the Harvard-MPQ Center for Quantum Optics and Air Force Office of Scientific Research - Multidisciplinary University Research Initiative (AFOSR-MURI) Grant No. FA95501610323. This research used resources of the National Energy Research Scientific Computing Center (NERSC), a U.S. Department of Energy Office of Science User Facility operated under Contract No. DE-AC02-05CH11231. J. K. acknowledges funding from Hector Fellow Academy and support by the Max Planck Harvard Research Center for Quantum Optics (MPHQ). E. D. and Y. W. acknowledge support from Harvard-MIT CUA, Harvard-MPQ Center, ARO Grant No. W911NF-20-1-0163, and the National Science Foundation through Grant No. OAC-1934714 and under Grant No. DMR-2038011.

[1] P. A. Lee, N. Nagaosa, and X.-G. Wen, Doping a mott insulator: Physics of high-temperature superconductivity, Rev. Mod. Phys. **78**, 17 (2006).

[2] B. Keimer, S. A. Kivelson, M. R. Norman, S. Uchida, and J. Zaanen, From quantum matter to high-temperature superconductivity in copper oxides, Nature (London) **518**, 179 (2015).

[3] F. C. Zhang and T. M. Rice, Effective hamiltonian for the superconducting cu oxides, Phys. Rev. B **37**, 3759 (1988).

[4] S. Schmitt-Rink, C. M. Varma, and A. E. Ruckenstein, Spectral Function of Holes in a Quantum Antiferromagnet, Phys. Rev. Lett. **60**, 2793 (1988).

[5] B. I. Shraiman and E. D. Siggia, Mobile Vacancies in a Quantum Heisenberg Antiferromagnet, Phys. Rev. Lett. **61**, 467 (1988).

[6] C. L. Kane, P. A. Lee, and N. Read, Motion of a single hole in a quantum antiferromagnet, Phys. Rev. B **39**, 6880 (1989).

[7] S. Sachdev, Hole motion in a quantum néel state, Phys. Rev. B **39**, 12232 (1989).

[8] A. Auerbach and B. E. Larson, Small-Polaron Theory of Doped Antiferromagnets, Phys. Rev. Lett. **66**, 2262 (1991).

[9] Z. Liu and E. Manousakis, Spectral function of a hole in the t-j model, Phys. Rev. B **44**, 2414 (1991).

[10] G. Martinez and P. Horsch, Spin polarons in the t-j model, Phys. Rev. B **44**, 317 (1991).

[11] M. Brunner, F. F. Assaad, and A. Muramatsu, Single-hole dynamics in the $t-j$ model on a square lattice, Phys. Rev. B **62**, 15480 (2000).

[12] A. S. Mishchenko, N. V. Prokof'ev, and B. V. Svistunov, Single-hole spectral function and spin-charge separation in the $t-j$ model, Phys. Rev. B **64**, 033101 (2001).

[13] S. R. White and I. Affleck, Density matrix renormalization group analysis of the nagaoka polaron in the two-dimensional $t-j$ model, Phys. Rev. B **64**, 024411 (2001).

[14] J. Koepsell, J. Vijayan, P. Sompet, F. Grusdt, T. A. Hilker, E. Demler, G. Salomon, I. Bloch, and C. Gross, Imaging magnetic polarons in the doped fermi-hubbard model, Nature (London) **572**, 358 (2019).

[15] F. Grusdt, A. Bohrdt, and E. Demler, Microscopic spinon-chargon theory of magnetic polarons in the $t-j$ model, Phys. Rev. B **99**, 224422 (2019).

[16] E. Blomquist and J. Carlström, Ab initio description of magnetic polarons in a mott insulator, arXiv:1912.08825.

[17] T. Giamarchi, *Quantum Physics in One Dimension* (Oxford University Press, Oxford, 2003).

[18] C. Kim, A. Y. Matsuura, Z.-X. Shen, N. Motoyama, H. Eisaki, S. Uchida, T. Tohyama, and S. Maekawa, Observation of Spin-Charge Separation in One-Dimensional $srcuo_2$, Phys. Rev. Lett. **77**, 4054 (1996).

[19] M. Sing, U. Schwingenschlögl, R. Claessen, P. Blaha, J. M. P. Carmelo, L. M. Martelo, P. D. Sacramento, M. Dressel, and C. S. Jacobsen, Electronic structure of the quasi-one-dimensional organic conductor ttf-tcnq, Phys. Rev. B **68**, 125111 (2003).

[20] J. Vijayan, P. Sompet, G. Salomon, J. Koepsell, S. Hirthe, A. Bohrdt, F. Grusdt, I. Bloch, and C. Gross, Time-resolved observation of spin-charge deconfinement in fermionic Hubbard chains, Science **367**, 186 (2020).

[21] R. J. Birgeneau, C. Stock, J. M. Tranquada, and K. Yamada, Magnetic neutron scattering in hole doped cuprate superconductors, J. Phys. Soc. Jpn. **75**, 111003 (2006).

[22] L. J. P. Ament, M. van Veenendaal, T. P. Devereaux, J. P. Hill, and J. van den Brink, Resonant inelastic x-ray scattering studies of elementary excitations, Rev. Mod. Phys. **83**, 705 (2011).

[23] S. Vig, A. Kogar, M. Mitrano, A. A. Husain, V. Mishra, M. S. Rak, L. Venema, P. D. Johnson, G. D. Gu, E. Fradkin, M. R. Norman, and P. Abbamonte, Measurement of the dynamic charge response of materials using low-energy, momentum-resolved electron energy-loss spectroscopy (M-EELS), SciPost Phys. **3**, 026 (2017).

[24] W. S. Bakr, J. I. Gillen, A. Peng, S. Foelling, and M. Greiner, A quantum gas microscope for detecting single atoms in a hubbard-regime optical lattice, Nature (London) **462**, 74 (2009).

[25] J. F. Sherson, C. Weitenberg, M. Endres, M. Cheneau, I. Bloch, and S. Kuhr, Single-atom-resolved fluorescence imaging of an atomic mott insulator, Nature (London) **467**, 68 (2010).

[26] M. F. Parsons, F. Huber, A. Mazurenko, C. S. Chiu, W. Setiawan, K. Wooley-Brown, S. Blatt, and M. Greiner, Site-Resolved Imaging of Fermionic ^{6}Li in an Optical Lattice, Phys. Rev. Lett. **114**, 213002 (2015).

[27] L. W. Cheuk, M. A. Nichols, M. Okan, T. Gersdorf, V. V. Ramasesh, W. S. Bakr, T. Lompe, and M. W. Zwierlein, Quantum-Gas Microscope for Fermionic Atoms, Phys. Rev. Lett. **114**, 193001 (2015).

[28] A. Omran, M. Boll, T. A. Hilker, K. Kleinlein, G. Salomon, I. Bloch, and C. Gross, Microscopic Observation of Pauli Blocking in Degenerate Fermionic Lattice Gases, Phys. Rev. Lett. **115**, 263001 (2015).

[29] G. J. A. Edge, R. Anderson, D. Jervis, D. C. McKay, R. Day, S. Trotzky, and J. H. Thywissen, Imaging and addressing of individual fermionic atoms in an optical lattice, Phys. Rev. A **92**, 063406 (2015).

[30] E. Haller, J. Hudson, A. Kelly, D. A. Cotta, B. Peaudecerf, G. D. Bruce, and S. Kuhr, Single-atom imaging of fermions in a quantum-gas microscope, Nat. Phys. **11**, 738 (2015).

[31] D. Leibfried, R. Blatt, C. Monroe, and D. Wineland, Quantum dynamics of single trapped ions, Rev. Mod. Phys. **75**, 281 (2003).

[32] T. Schweigler, V. Kasper, S. Erne, I. Mazets, B. Rauer, F. Cataldini, T. Langen, T. Gasenzer, J. Berges, and J. Schmiedmayer, Experimental characterization of a quantum many-body system via higher-order correlations, Nature (London) **545**, 323 (2017).

[33] M. Endres, M. Cheneau, T. Fukuhara, C. Weitenberg, P. Schauss, C. Gross, L. Mazza, M. C. Banuls, L. Pollet, I. Bloch, and S. Kuhr, Observation of correlated particle-hole pairs and string order in low-dimensional mott insulators, Science **334**, 200 (2011).

[34] M. Boll, T. A. Hilker, G. Salomon, A. Omran, J. Nespolo, L. Pollet, I. Bloch, and C. Gross, Spin- and density-resolved microscopy of antiferromagnetic correlations in fermi-hubbard chains, Science **353**, 1257 (2016).

[35] A. Lukin, M. Rispoli, R. Schittko, M. E. Tai, A. M. Kaufman, S. Choi, V. Khemani, J. Léonard, and M. Greiner, Probing entanglement in a many-body-localized system, Science **364**, 256 (2019).

[36] J. Koepsell, S. Hirthe, D. Bourgund, P. Sompet, J. Vijayan, G. Salomon, C. Gross, and I. Bloch, Robust Bilayer Charge-Pumping for Spin- and Density-Resolved Quantum Gas Microscopy, Phys. Rev. Lett. **125**, 010403 (2020).

[37] M. Prüfer, T. V. Zache, P. Kunkel, S. Lannig, A. Bonnin, H. Strobel, J. Berges, and M. K. Oberthaler, Experimental extraction of the quantum effective action for a non-equilibrium many-body system, Nat. Phys. **16**, 1012 (2020).

[38] T. V. Zache, T. Schweigler, S. Erne, J. Schmiedmayer, and J. Berges, Extracting the Field Theory Description of a Quantum Many-Body System from Experimental Data, Phys. Rev. X **10**, 011020 (2020).

[39] S. R. White and D. J. Scalapino, Hole and pair structures in the t-j model, Phys. Rev. B **55**, 6504 (1997).

[40] G. B. Martins, R. Eder, and E. Dagotto, Indications of spin-charge separation in the two-dimensional extended t-j model, Phys. Rev. B **60**, R3716 (1999).

[41] G. B. Martins, C. Gazza, J. C. Xavier, A. Feiguin, and E. Dagotto, Doped Stripes in Models for the Cuprates Emerging from the One-Hole Properties of the Insulator, Phys. Rev. Lett. **84**, 5844 (2000).

[42] G. B. Martins, J. C. Xavier, C. Gazza, M. Vojta, and E. Dagotto, Indications of spin-charge separation at short distance and stripe formation in the extended t-j model on ladders and planes.

[43] S. Huber, F. Grusdt, and M. Punk, Signatures of correlated magnetic phases in the two-spin density matrix, Phys. Rev. A **99**, 023617 (2019).

[44] F. Grusdt, M. Kánasz-Nagy, A. Bohrdt, C. S. Chiu, G. Ji, M. Greiner, D. Greif, and E. Demler, Parton Theory of Magnetic Polarons: Mesonic Resonances and Signatures in Dynamics, Phys. Rev. X **8**, 011046 (2018).

[45] P. Beran, D. Poilblanc, and R. B. Laughlin, Evidence for composite nature of quasiparticles in the 2d t-j model, Nucl. Phys. **B473**, 707 (1996).

[46] R. B. Laughlin, Evidence for Quasiparticle Decay in Photoemission from Underdoped Cuprates, Phys. Rev. Lett. **79**, 1726 (1997).

[47] G. Baskaran, 3/2-fermi liquid: the secret of high-tc cuprates, arXiv:0709.0902.

[48] S. Sachdev, H. D. Scammell, M. S. Scheurer, and G. Tarnopolsky, Gauge theory for the cuprates near optimal doping, Phys. Rev. B **99**, 054516 (2019).

[49] Y. Wang, A. Bohrdt, J. Koepsell, E. Demler, and F. Grusdt, Higher-Order Spin-Hole Correlations around a Localized Charge Impurity, arXiv:2101.00721.

[50] See Supplemental Material at http://link.aps.org/supplemental/10.1103/PhysRevLett.126.026401 for the explicit definition of the connected correlator.

[51] H. Bruus and K. Flensberg, *Many-Body Quantum Theory in Condensed Matter Physics* (Oxford University Press, Oxford, 2004).

[52] Our code uses the TeNPy package [77,78]. We averaged over the six legs of the cylinder to speed up convergence of the considered higher-order correlator.

[53] A. Auerbach, *Interacting Electrons and Quantum Magnetism* (Springer, Berlin, 1998).

[54] A. L. Chernyshev and P. W. Leung, Holes in the $t-J_z$ model: A diagrammatic study, Phys. Rev. B **60**, 1592 (1999).

[55] C. S. Chiu, G. Ji, A. Bohrdt, M. Xu, M. Knap, E. Demler, F. Grusdt, M. Greiner, and D. Greif, String patterns in the doped Hubbard model, Science **365**, 251 (2019).

[56] A. Bohrdt, C. S. Chiu, G. Ji, M. Xu, D. Greif, M. Greiner, E. Demler, F. Grusdt, and M. Knap, Classifying snapshots of

the doped Hubbard model with machine learning, Nat. Phys. **15**, 921 (2019).
[57] P. W. Anderson, The resonating valence bond state in la2cuo4 and superconductivity, Science **235**, 1196 (1987).
[58] G. Baskaran, Z. Zou, and P. W. Anderson, The resonating valence bond state and high-tc superconductivity—A mean field theory, Solid State Commun. **63**, 973 (1987).
[59] C. Gros, Physics of projected wavefunctions, Ann. Phys. (N.Y.) **189**, 53 (1989).
[60] T. Giamarchi and C. Lhuillier, Dispersion relation of a single hole in the t-j model determined by a variational monte carlo method, Phys. Rev. B **47**, 2775 (1993).
[61] X.-G. Wen and P. A. Lee, Theory of Underdoped Cuprates, Phys. Rev. Lett. **76**, 503 (1996).
[62] A. Bohrdt, Eugene Demler, Frank Pollmann, Michael Knap, and Fabian Grusdt,Parton theory of arpes spectra in antiferromagnetic Mott insulators, Phys. Rev. B **102**, 035139 (2020).
[63] T. K. Lee and S. Feng, Doping dependence of antiferromagnetism in la_2cuo_4: A numerical study based on a resonating-valence-bond state, Phys. Rev. B **38**, 11809 (1988).
[64] B. D. Piazza, M. Mourigal, N. B. Christensen, G. J. Nilsen, P. Tregenna-Piggott, T. G. Perring, M. Enderle, D. F. McMorrow, D. A. Ivanov, and H. M. Ronnow, Fractional excitations in the square-lattice quantum antiferromagnet, Nat. Phys. **11**, 62 (2015).
[65] We used the same Monte Carlo code as in Ref. [55].
[66] A. Mazurenko, C. S. Chiu, G. Ji, M. F. Parsons, M. Kanasz-Nagy, R. Schmidt, F. Grusdt, E. Demler, D. Greif, and M. Greiner, A cold-atom Fermi-Hubbard antiferromagnet, Nature (London) **545**, 462 (2017).
[67] C. S. Chiu, G. Ji, A. Mazurenko, D. Greif, and M. Greiner, Quantum State Engineering of a Hubbard System with Ultracold Fermions, Phys. Rev. Lett. **120**, 243201 (2018).
[68] P. T. Brown, D. Mitra, E. Guardado-Sanchez, P. Schauss, S. S. Kondov, E. Khatami, T. Paiva, N. Trivedi, D. A. Huse, and W. S. Bakr, Spin-imbalance in a 2d Fermi-Hubbard system, Science **357**, 1385 (2017).
[69] H. V. Kruis, I. P. McCulloch, Z. Nussinov, and J. Zaanen, Geometry and the hidden order of Luttinger liquids: The universality of squeezed space, Phys. Rev. B **70**, 075109 (2004).
[70] T. A. Hilker, G. Salomon, F. Grusdt, A. Omran, M. Boll, E. Demler, I. Bloch, and C. Gross, Revealing hidden antiferromagnetic correlations in doped Hubbard chains via string correlators, Science **357**, 484 (2017).
[71] J. P. F. LeBlanc *et al.*, Solutions of the Two-Dimensional Hubbard Model: Benchmarks and Results from a Wide Range of Numerical Algorithms, Phys. Rev. X **5**, 041041 (2015).
[72] P. T. Brown, D. Mitra, E. Guardado-Sanchez, R. Nourafkan, A. Reymbaut, C.-D. Hebert, S. Bergeron, A.-M. S. Tremblay, J. Kokalj, D. A. Huse, P. Schauß, and W. S. Bakr, Bad metallic transport in a cold atom Fermi-Hubbard system, Science **363**, 379 (2019).
[73] A. Bohrdt, F. Grusdt, and M. Knap, Dynamical formation of a magnetic polaron in a two-dimensional quantum antiferromagnet, New J. Phys. **22**, 123023 (2020).
[74] C. Hubig, A. Bohrdt, M. Knap, F. Grusdt, and I. Cirac. Evaluation of time-dependent correlators after a local quench in ipeps: Hole motion in the t-j model, SciPost Phys. **8**, 021 (2020).
[75] G. Ji, M. Xu, L. H. Kendrick, C. S. Chiu, J. C. Brüggenjürgen, D. Greif, A. Bohrdt, F. Grusdt, E. Demler, M. Lebrat, and M. Greiner, Dynamical interplay between a single hole and a Hubbard antiferromagnet, arXiv:2006.06672v1.
[76] T. Fukuhara, A. Kantian, M. Endres, M. Cheneau, P. Schauss, S. Hild, D. Bellem, U. Schollwoeck, T. Giamarchi, C. Gross, I. Bloch, and S. Kuhr, Quantum dynamics of a mobile spin impurity, Nat. Phys. **9**, 235 (2013).
[77] The code is available online at https://github.com/tenpy/tenpy/, and the documentation can be found at https://tenpy.readthedocs.io.
[78] J. Hauschild and F. Pollmann, Efficient Numerical Simulations with Tensor Networks: Tensor Network Python (TeNPy), SciPost Phys. Lect. Notes **5** (2018).